



Co-overproducing Rubisco and Rubisco activase enhances photosynthesis in the optimal temperature range in rice

Mao Suganami,¹ Yuji Suzuki,² Youshi Tazoe,^{1,†} Wataru Yamori ³ and Amane Makino ^{1,*‡}

1 Graduate School of Agricultural Science, Tohoku University, Sendai 980-8572, Japan

2 Faculty of Agriculture, Iwate University, Morioka, Iwate 020-8550, Japan

3 Graduate School of Agricultural Life Sciences, The University of Tokyo, Tokyo 113-8657, Japan

*Author for communication: amanemakino@tohoku.ac.jp

†Present address: Faculty of Agri-Food Science, Niigata Agro-Food University, Niigata 959-2702, Japan.

‡Senior author.

A.M. and Y.S. conceived and designed the experiments. M.S. performed most of the experiments. M.S., Y.S., Y.T., W.Y., and A.M. analyzed the data. M.S., Y.S., and A.M. wrote the article.

The author responsible for distribution of materials integral to the findings presented in this article in accordance with the policy described in the Instructions for Authors (<https://academic.oup.com/plphys>) is: Amane Makino (amanemakino@tohoku.ac.jp).

Abstract

Rubisco limits C₃ photosynthesis under some conditions and is therefore a potential target for improving photosynthetic efficiency. The overproduction of Rubisco is often accompanied by a decline in Rubisco activation, and the protein ratio of Rubisco activase (RCA) to Rubisco (RCA/Rubisco) greatly decreases in Rubisco-overproducing plants (*RBCS-ox*). Here, we produced transgenic rice (*Oryza sativa*) plants co-overproducing both Rubisco and RCA (*RBCS-RCA-ox*). Rubisco content in *RBCS-RCA-ox* plants increased by 23%–44%, and RCA/Rubisco levels were similar or higher than those of wild-type plants. However, although the activation state of Rubisco in *RBCS-RCA-ox* plants was enhanced, the rates of CO₂ assimilation at 25°C in *RBCS-RCA-ox* plants did not differ from that of wild-type plants. Alternatively, at a moderately high temperature (optimal range of 32°C–36°C), the rates of CO₂ assimilation in *RBCS-ox* and *RBCS-RCA-ox* plants were higher than in wild-type plants under conditions equal to or lower than current atmospheric CO₂ levels. The activation state of Rubisco in *RBCS-RCA-ox* remained higher than that of *RBCS-ox* plants, and activated Rubisco content in RCA overproducing, *RBCS-ox*, *RBCS-RCA-ox*, and wild-type plants was highly correlated with the initial slope of CO₂ assimilation against intercellular CO₂ pressures (A:Ci) at 36°C. Thus, a simultaneous increase in Rubisco and RCA contents leads to enhanced photosynthesis within the optimal temperature range.

Introduction

Due to global human population growth, there is an increase in food demand. However, the rate of increase in crop productivity is insufficient for prospective food demand over the coming decades (Long et al., 2015). In addition, accelerated global warming will negatively affect crop productivity (IPCC,

2013). Therefore, there is a need for improvement of crop productivity under near-future climatic conditions. Increasing the photosynthetic efficiency in crop plants is considered to be one of the promising strategies to increase crop productivity (e.g. Makino, 2011; Ort et al., 2015). According to the biochemical model for C₃ photosynthesis by Farquhar et al.

(1980), photosynthetic rate is either limited by the capacity of ribulose-1,5-bisphosphate (RuBP) carboxylase/oxygenase (Rubisco; E.C. 4.1.1.39) to consume RuBP or by the capacity of the chloroplast electron transport to regenerate RuBP. Based on this model, light-saturated photosynthesis is limited by the capacity of Rubisco below current atmospheric CO₂ concentrations (Evans, 1986; Makino et al., 1988). Transgenic plants with decreased Rubisco content exhibit reduced photosynthetic rates parallel to the decreased Rubisco content (Quick et al., 1991; Hudson et al., 1992; Furbank et al., 1996; Makino et al., 1997). In addition, a recent study analyzing the limiting factor of temperature-dependent photosynthesis suggests that at high temperatures Rubisco strongly limits photosynthesis (Busch and Sage, 2017). Therefore, Rubisco has been considered as an attractive target for enhancing the photosynthetic capacity (Carmo-Silva et al., 2015; von Caemmerer, 2020).

In our previous study, we produced transgenic rice (*Oryza sativa*) plants with a 30% increase in the Rubisco content by the overexpression of the *RBCS* gene (*RBCS*-ox plants; Suzuki et al., 2007). In growth chambers, *RBCS*-ox rice plants exhibit higher biomass production under CO₂-limited conditions (Sudo et al., 2014). In isolated paddy field conditions, *RBCS*-ox rice plants show higher grain yields than that of wild-type (WT) plants under sufficient nitrogen fertilization (Yoon et al., 2020). However, the overproduction of Rubisco is accompanied by a decline in Rubisco activation (Makino and Sage, 2007; Suzuki et al., 2009; Suganami et al., 2018). Therefore, the photosynthetic rate did not necessarily increase in Rubisco-overproducing rice plants (Suzuki et al., 2009; Suganami et al., 2018). Recently, similar phenomena have been reported in Rubisco-overproducing maize (*Zea mays*) plants (Salesse-Smith et al., 2018). Thus, a decline in the activation state of Rubisco in Rubisco-overproducing plants may be one of the factors that hinder the improvement of photosynthesis in crops.

To become catalytically competent, Rubisco must be carbamylated and stabilized by the subsequent binding of Mg²⁺. However, sugar phosphates, including the substrate RuBP, carboxyarabinitol 1-phosphate (a nocturnal metabolite), and some misfire products, bind to noncarbamylated or carbamylated Rubisco and inhibit enzymic activity (Parry et al., 2008). Rubisco activase (RCA) is a member of the AAA+ family of proteins, which promotes the activation of Rubisco by facilitating the ATP-dependent removal of inhibitory sugar phosphates and carbamylation of Rubisco (Portis, 2003; Bracher et al., 2017). Most plants, including rice, contain two isoforms of RCA—redox-sensitive large and redox-insensitive small isoforms (Zhang and Portis, 1999; Zhang et al., 2002). Changes in redox status and ATP/ADP ratio in the chloroplast regulate the activity of RCA (Carmo-Silva and Salvucci, 2013). In *RBCS*-ox plants, ATP concentrations and ATP/ADP ratios during steady-state photosynthesis are similar to those in WT plants (Suzuki et al., 2012). In addition, electron transport rate through PSII (ETR_{II}) and PSI (ETR_I) in *RBCS*-ox plants does not change in comparison to

WT plants (Wada et al., 2018). These results indicate that ATP supply and electron transport activity are adequate for the activation of Rubisco. Alternatively, RCA content and the protein ratio of RCA to Rubisco (RCA/Rubisco) decrease in *RBCS*-ox plants by 10%–20% and 30%–40%, respectively (Suganami et al., 2018). Studies on transgenic plants with moderately suppressed RCA reveal that RCA is sufficient for maintaining Rubisco activation and photosynthesis (Mate et al., 1996; Eckardt et al., 1997; Masumoto et al., 2012; Yamori et al., 2012), but the activation state of Rubisco increases in transgenic rice plants with overproduced RCA (*RCA*-ox plants; Suganami et al., 2020). Similar results have also been observed in transgenic rice with overproduced barley (*Hordeum vulgare*) or maize RCA (Fukayama et al., 2012; Yamori et al., 2012). Therefore, we hypothesized the overproduction of RCA would restore a decline in Rubisco activation in *RBCS*-ox plants.

In this study, we produced transgenic rice plants with co-overproduced Rubisco and RCA (*RBCS*-*RCA*-ox plants) and examined whether the overproduction of RCA restores a decline in Rubisco activation in *RBCS*-ox plants. Then, we measured the rate of CO₂ assimilation under conditions of high irradiance and different CO₂ levels. Finally, we investigated the rate of CO₂ assimilation and the activation state of Rubisco at a moderately high temperature within the optimal temperature range (32°C–36°C).

Results

Rice has five *RBCS* genes (*RBCS1*–*RBCS5*) in the nuclear genome, and four out of five are mainly expressed in leaf blades (Suzuki et al., 2007). Rubisco-overproducing rice plants (*RBCS*-ox plants) were produced by transformation with *RBCS2* cDNA under the control of the *RBCS2* promoter (Suzuki et al., 2007). Rice contains large and small isoforms of RCA that arise from one nuclear gene via alternative splicing (To et al., 1999). *RCA*-overproducing rice plants (*RCA*-ox plants) were transformed with the cDNA of the small form of *RCA* under the control of the *RBCS2* promoter or the *RCA* promoter (Suganami et al., 2020). In the present study, we crossed two lines of *RBCS*-ox plants with four lines of *RCA*-ox plants and obtained five individual lines co-overproducing Rubisco and *RCA* (*RBCS*-*RCA*-ox plants; summarized in Supplemental Table S1). We used three lines of *RBCS*-*RCA*-ox plants (*RBCS*-*RCA*-ox 1, 2, and 3), which were derived from the Sr26-8 line of *RBCS*-ox plants. F2 and F3 progenies homozygous for both *RBCS* and *RCA* transgenes were selected. To confirm the common impact of the Rubisco overproduction, we also examined the remaining two lines (*RBCS*-*RCA*-ox 4 and 5), which were derived from another line of *RBCS*-ox plants (Sr35-4; Supplemental Figures S1 and S2).

All plants were grown hydroponically at 26°C/20°C day/night temperature in an environmentally controlled growth chamber. The experiments were conducted on the uppermost, fully expanded leaves of the 63- to 77-d-old plants.

Rubisco, RCA, and leaf N content in transgenic plants with co-overproduced Rubisco and RCA

Total leaf nitrogen (leaf-N) content did not differ, irrespective of the genotype (Figure 1A). The Rubisco content increased by 51% in *RBCS*-ox plants and by 23%, 44%, and 30% in *RBCS*-*RCA*-ox 1, 2, and 3 plants, respectively, compared with WT plants (Figure 1B). The content of the small isoform RCA (RCA_S) tended to decrease in *RBCS*-ox plants but increased by 42, 120, and 33% in *RBCS*-*RCA*-ox 1, 2, and 3 plants, respectively (Figure 1C). The ratio of Rubisco to total leaf-N content (Rubisco-N) was significantly higher in *RBCS*-ox plants and the three *RBCS*-*RCA*-ox plants than in WT plants, and RCA_S -N significantly increased in *RBCS*-*RCA*-ox plants compared with WT and *RBCS*-ox plants (Figure 1, D and E). Similar results were obtained with the other two lines (*RBCS*-*RCA*-ox 4 and 5; Supplemental Figure S1). The protein ratio of RCA to Rubisco content ($RCA/Rubisco$), which was calculated from Figure 1, B and C, was significantly lower in *RBCS*-ox plants, while that in *RBCS*-*RCA*-ox 1 and 3 plants was similar to the ratio of WT plants and that in *RBCS*-*RCA*-ox 2 plants was higher than in WT plants (Figure 1F). The typical examples of the detection images of Rubisco and RCA using sodium dodecyl sulphate–polyacrylamide gel electrophoresis (SDS–PAGE) are shown in Supplemental Figure S1.

Levels of mRNA of total *RBCS* (sum of four genes, *RBCS*2, 3, 4, and 5) and *RBCL* were 118% and 50% higher in *RBCS*-ox plants than in WT plants, respectively (Figure 2, A and B). These results were consistent with our previous studies (Suzuki et al., 2007, 2009; Suzuki and Makino, 2012). In *RBCS*-*RCA*-ox plants, the mRNA levels of total *RBCS* and *RBCL* were also 65%–78% and 26%–56% higher than those of WT plants, respectively (Figure 2, A and B). The mRNA levels of *RCA* were 28% lower in *RBCS*-ox plants than in WT plants but 39 and 156% higher in *RBCS*-*RCA*-ox 1 and 2 plants, respectively (Figure 2C).

Rubisco activation and rates of CO₂ assimilation at 25°C in transgenic plants with co-overproduced Rubisco and RCA

The activation state of Rubisco under saturated light conditions significantly decreased in *RBCS*-ox plants but was similar in the three lines of *RBCS*-*RCA*-ox plants compared to the WT plants (Figure 3). These results indicate that a decline in Rubisco activation in *RBCS*-ox plants was restored by the overproduction of RCA. However, the rate of CO₂ assimilation measured at 25°C did not increase in the three lines of *RBCS*-*RCA*-ox plants, irrespective of CO₂ partial pressures (Figure 4A). Similar results were also observed with the *RBCS*-*RCA*-ox 4 and 5 plants (Supplemental Figure S2).

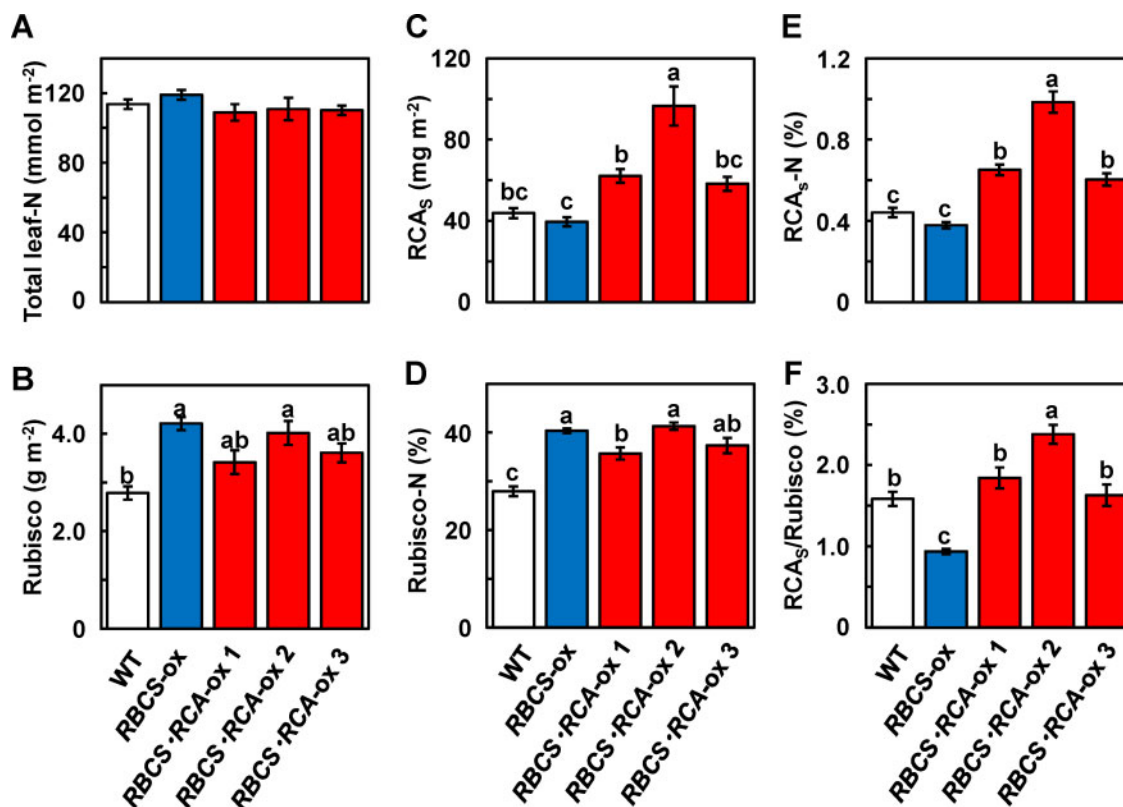


Figure 1 Rubisco, RCA and leaf-N contents in transgenic plants. (A) Total leaf-N; (B) Rubisco; (C) RCA small form (RCA_S) contents per unit of leaf area; (D) N allocation to Rubisco (Rubisco-N); (E) N allocation to RCA_S (RCA_S -N) and (F) the protein ratio of RCA_S to Rubisco ($RCA_S/Rubisco$) in the uppermost, fully expanded leaves. The white, blue, and red bars indicate WT, *RBCS*-ox, and *RBCS*-*RCA*-ox plants, respectively. Data are presented as means \pm SE ($n = 4-6$). Statistical analysis was conducted using ANOVA with a post hoc Tukey–Kramer HSD test. Different letters indicate statistical differences among the genotypes ($P < 0.05$).

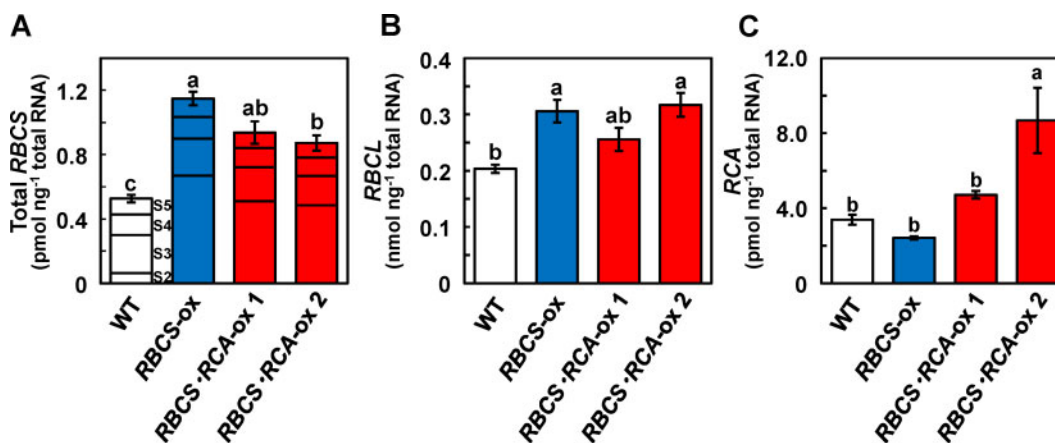


Figure 2 The mRNA levels of total RBCS, RBCL, and RCA in transgenic plants. The mRNA levels of: (A) total RBCS; (B) RBCL in expanding leaves; and (C) RCA in fully expanded leaves on a total RNA basis. In total RBCS, each bar was divided into four parts, which indicate the mRNA levels of four genes of the RBCS multigene family, RBCS2, 3, 4, and 5, respectively, from the bottom to the top. The mRNA level of RBCS1 was negligible (Suzuki et al., 2007). The white, blue, and red bars indicate WT, RBCS-ox, and RBCS-RCA-ox plants, respectively. Data are presented as means \pm SE ($n = 3-4$). Statistical analysis was conducted using ANOVA with a post hoc Tukey–Kramer HSD test. Different letters indicate statistical differences among the genotypes ($P < 0.05$).

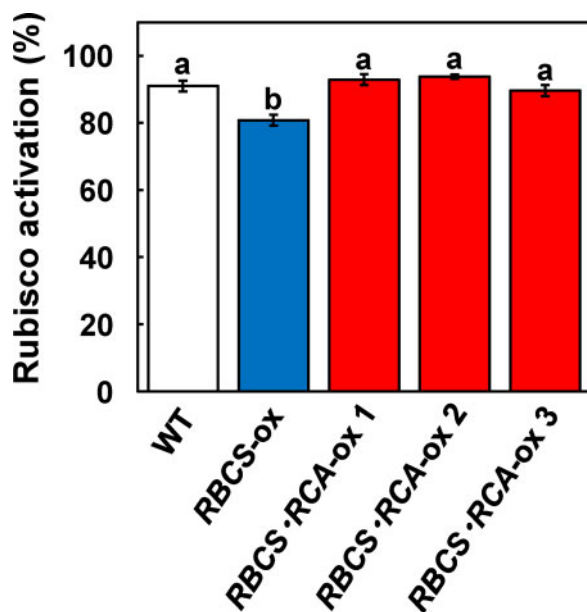


Figure 3 Rubisco activation at 25°C in transgenic plants. The activation state of Rubisco was measured in the uppermost, fully expanded leaves at a leaf temperature of 25°C, an irradiance of 1,500- μ mol quanta $m^{-2} s^{-1}$, and an atmospheric CO₂ partial pressure (C_a) of 40 Pa. The white, blue, and red bars indicate WT, RBCS-ox, and RBCS-RCA-ox plants, respectively. Data are presented as means \pm SE ($n = 3-6$). Statistical analysis was conducted using ANOVA with a post hoc Tukey–Kramer HSD test. Different letters indicate statistical differences among the genotypes ($P < 0.05$).

The analysis of CO₂ assimilation as a function of intercellular CO₂ pressures ($A:C_i$ curve) showed the tendency toward a decrease in CO₂ assimilation in RBCS-ox and RBCS-RCA-ox plants at elevated CO₂ levels (Figure 4B), but there was no difference in the initial slope of $A:C_i$ curves among genotypes (Figure 4C). Maximum rates of electron transport

(J_{max}) and of RuBP carboxylation (V_{cmax}) were calculated using the gas exchange data (Figure 4) according to the photosynthetic biochemical model (von Caemmerer and Farquhar, 1981). Although the calculated J_{max} tended to slightly decrease in some RBCS-RCA-ox plants, it did not statistically differ among genotypes (Table 1). In addition, the rates at 40 Pa CO₂ (A_i) predicted from the calculated J_{max} in all genotypes were comparable to the measured rates of CO₂ assimilation at 40 Pa CO₂ (A_{mes}), respectively. These results suggest that the rate of CO₂ assimilation at atmospheric CO₂ partial pressures in RBCS-RCA-ox plants is limited by the electron-transport rate. Therefore, it was considered that the rate of CO₂ assimilation at 40 Pa CO₂ in RBCS-RCA-ox plants did not increase. In addition, no difference in V_{cmax} (Table 1) as well as in the initial slope of $A:C_i$ (Figure 4C) indicated that CO₂ assimilation in RBCS-RCA-ox plants did not increase, even under CO₂-limited conditions where Rubisco limits photosynthesis.

Co-overproduction of Rubisco and RCA increased the rates of CO₂ assimilation at moderately high temperatures

Our previous studies on the temperature response of photosynthesis in rice show that the maximum rates of CO₂ assimilation in rice are observed in a wide temperature range of 25°C–37°C (Makino and Sage, 2007; Nagai and Makino, 2009). In addition, the optimal temperature in RBCS-ox rice plants tends to shift toward high temperature ranges (Makino and Sage, 2007). Therefore, we measured the rate of CO₂ assimilation at moderately high temperatures (32°C and 36°C) in WT, RCA-ox, RBCS-ox, and RBCS-RCA-ox plants (transgenic line with the highest Rubisco and RCA contents, see Figure 1). Whereas there was no difference in the rate of CO₂ assimilation at 25°C among genotypes under any CO₂ conditions, the rate of CO₂ assimilation at 32°C in

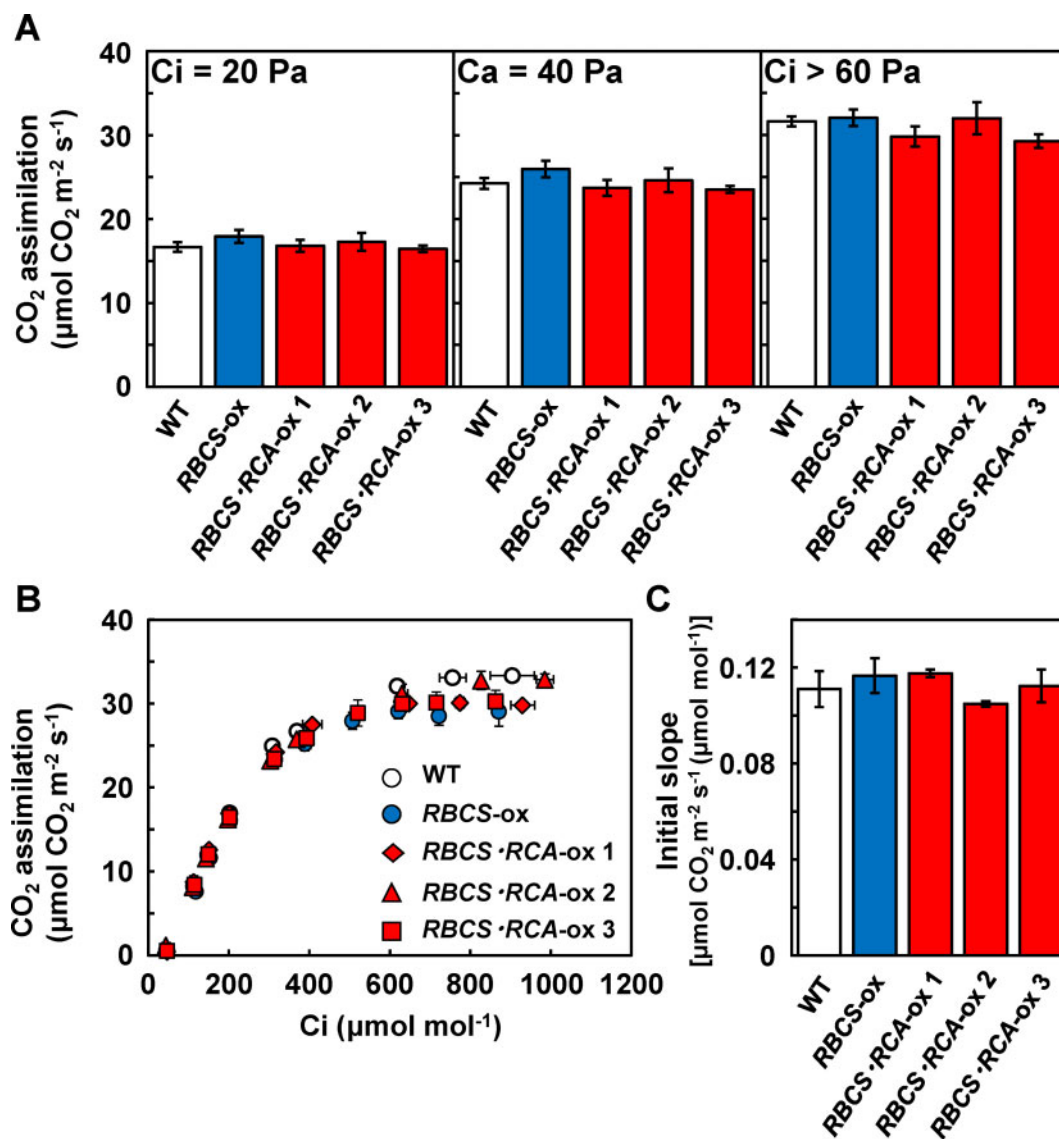


Figure 4 Rates of CO₂ assimilation at 25°C in transgenic plants. **(A)** The rate of CO₂ assimilation per unit of leaf area in the uppermost, fully expanded leaves measured with an LI-6400XT at a leaf temperature of 25°C, an irradiance of 1,500-μmol quanta m⁻² s⁻¹, and different CO₂ partial pressures (intercellular CO₂ partial pressure, Ci, of 20 Pa (Ci = 20 Pa), Ca = 40 Pa, and Ci > 60 Pa). The white, blue, and red bars indicate WT, RBCS-ox, and RBCS-RCA-ox plants, respectively. Data are presented as means ± SE (n = 4–6). **(B)** The rates of CO₂ assimilation as a function of Ci (A:Ci curve). The white circles, blue circles, red diamonds, red triangles, and red squares indicate WT, RBCS-ox, RBCS-RCA-ox 1, 2, and 3 plants, respectively. Data are presented as means ± SE (n = 3–4). **(C)** Initial slope of CO₂ assimilation against Ci. The slope was calculated from the data of **(B)**. In **(A)** and **(C)**, statistical analysis was conducted using ANOVA with a post hoc Tukey–Kramer HSD test. Different letters indicate statistical differences among the genotypes (P < 0.05).

Table 1 J_{max}, V_{cmax} and calculated/measured CO₂ assimilation at Ca = 40 Pa in transgenic plants

Rate	WT	RBCS-ox	RBCS-RCA-ox 1	RBCS-RCA-ox 2	RBCS-RCA-ox 3
J _{max} (μmol m ⁻² s ⁻¹)	162.3 ± 3.0	164.5 ± 4.8	152.6 ± 6.4	162.8 ± 9.1	150.2 ± 3.8
V _{cmax} (μmol m ⁻² s ⁻¹)	94.4 ± 8.5	102.8 ± 8.0	101.9 ± 1.7	86.5 ± 1.2	96.4 ± 7.0
A _j (μmol CO ₂ m ⁻² s ⁻¹)	26.3 ± 0.5	26.4 ± 0.8	24.6 ± 0.6	26.0 ± 1.5	24.2 ± 0.6
A _{mes} (μmol CO ₂ m ⁻² s ⁻¹)	24.3 ± 0.7	26.0 ± 1.0	23.7 ± 1.0	24.6 ± 3.0	23.7 ± 1.0

J_{max} and V_{cmax} were calculated from the data of CO₂ assimilation at Ci > 60 Pa and initial slope of A:Ci curve in **Figure 4**, respectively. CO₂ assimilation limited by RuBP regeneration (A_j) at Ca = 40 Pa was calculated from **Equation (5)** in the Materials and methods section. Measured CO₂ assimilation (A_{mes}) was taken from data in **Figure 4A**. Data are presented as means ± SE (n = 3–6). Statistical analysis was conducted using ANOVA with a post hoc Tukey–Kramer HSD test. Different letters indicate statistical differences among the genotypes (P < 0.05).

RBCS-RCA-ox 2 plants tended to be higher than in WT and RCA-ox plants under conditions of $C_i = 20$ Pa and $C_a = 40$ Pa (Figure 5). In addition, the rate of CO_2 assimilation at $36^\circ C$ in RBCS-RCA-ox 2 plants was significantly higher than that of WT plants by 21 and 14% under conditions of $C_i = 20$ Pa and $C_a = 40$ Pa, respectively (Figure 5A). When the rate of CO_2 assimilation relative to that at $25^\circ C$ was calculated (Figure 5B), there were statistically significant increases in the rate of CO_2 assimilation at $32^\circ C$ in RBCS-ox plants compared to WT plants under conditions of $C_i = 20$ Pa and $C_a = 40$ Pa.

Rubisco content in RBCS-ox and RBCS-RCA-ox 2 plants significantly increased compared to that in WT plants, and that in RCA-ox plants was slightly lower (Figure 6A). The activation state of Rubisco in RCA-ox plants remained at high levels even at high temperatures. Alternatively, the activation state of Rubisco in WT, RBCS-ox, and RBCS-RCA-ox 2

plants decreased with increasing temperature. The activation state of Rubisco in RBCS-RCA-ox 2 plants was similar to that of WT plants and higher than that of RBCS-ox plants at any temperature (Figure 6B). These results indicate that the overproduction of RCA is effective in preventing partial deactivation of Rubisco caused by the overproduction of Rubisco even at high temperatures.

We conducted the A: C_i curve analysis at $36^\circ C$ (Figure 7). From low to normal CO_2 partial pressures, CO_2 assimilation in RBCS-ox and RBCS-RCA-ox 2 plants was higher than in WT plants. Alternatively, at elevated CO_2 levels, the rate of CO_2 assimilation in RBCS-ox and RBCS-RCA-ox 2 plants did not differ from that of WT plants (Figure 7A). The initial slope of the A: C_i curve in RBCS-RCA-ox 2 plants was the highest among genotypes and the incremental ratio of RBCS-RCA-ox 2 plants was 33% compared to WT plants (Figure 7B).

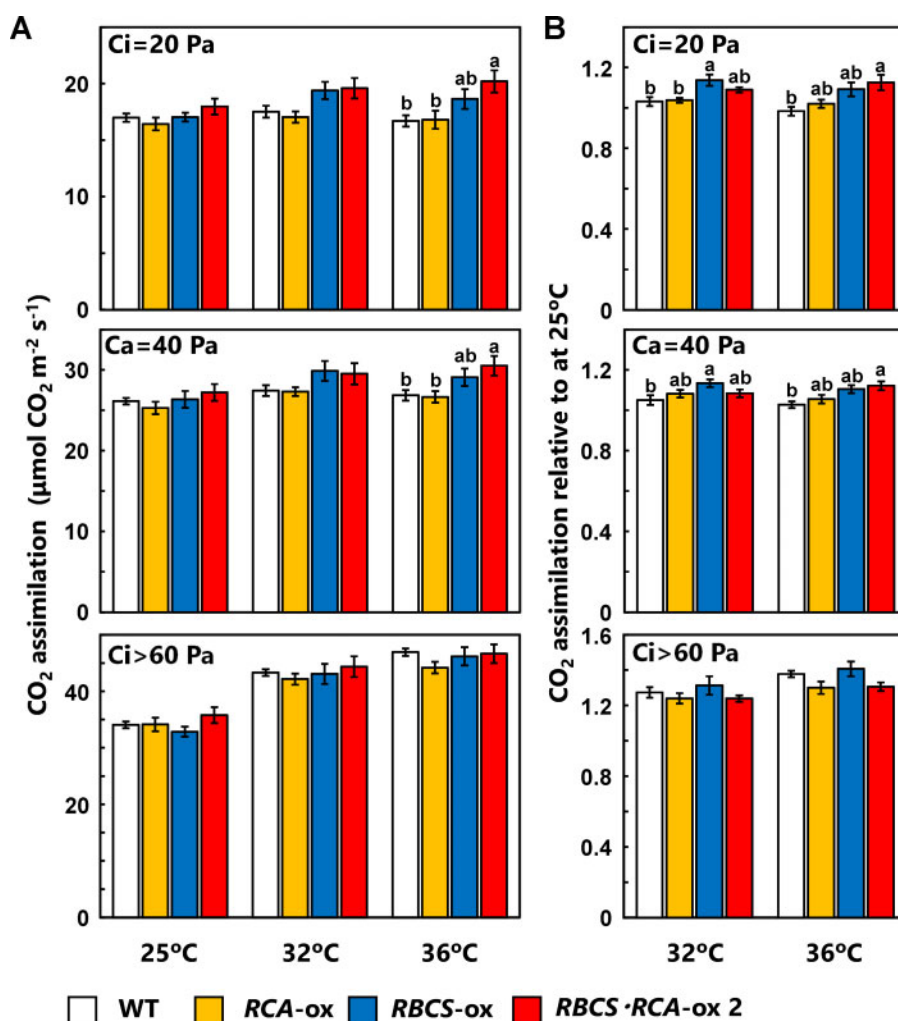


Figure 5 Rates of CO_2 assimilation at $25^\circ C$, $32^\circ C$, and $36^\circ C$ in transgenic plants. (A) The rate of CO_2 assimilation per unit of leaf area in the uppermost, fully expanded leaves measured with an LI-6800 at an irradiance of $1,500\text{-}\mu mol$ quanta $m^{-2} s^{-1}$, different CO_2 partial pressures ($C_i = 20$ Pa, $C_a = 40$ Pa, and $C_i > 60$ Pa) and different leaf temperatures (25, 32, and $36^\circ C$). (B) The rate of CO_2 assimilation at $32^\circ C$ and $36^\circ C$ relative to that at $25^\circ C$. The white, orange, blue, and red bars indicate WT, RCA-ox, RBCS-ox, and RBCS-RCA-ox 2 plants, respectively. Data are presented as means \pm SE ($n = 6\text{--}7$). Statistical analysis was conducted using ANOVA with a post hoc Tukey–Kramer HSD test. Different letters indicate statistical differences among the genotypes ($P < 0.05$).

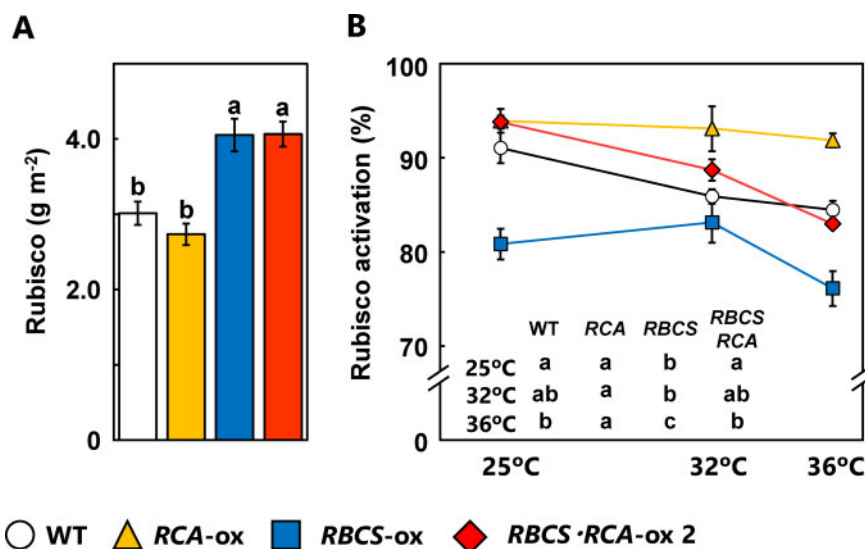


Figure 6 Rubisco content and Rubisco activation at 25, 32, and 36°C in transgenic plants. (A) Rubisco content per unit of leaf area in the uppermost, fully expanded leaves. Data are presented as means \pm SE ($n = 6-7$). (B) The activation state of Rubisco was measured in the uppermost, fully expanded leaves at an irradiance of $1,500\text{-}\mu\text{mol quanta m}^{-2}\text{ s}^{-1}$, an ambient CO_2 partial pressure ($C_a = 40\text{ Pa}$) and different leaf temperatures (25, 32, and 36°C). Data are presented as means \pm SE ($n = 3-6$). The white circles, orange triangles, blue squares, and red diamonds indicate WT, RCA-ox, RBCS-ox, and RBCS-RCA-ox 2 plants, respectively. Statistical analysis was conducted using ANOVA with a post hoc Tukey-Kramer HSD test. Different letters indicate statistical differences among the genotypes ($P < 0.05$).

We defined “Rubisco content” multiplied by “Rubisco activation” as “activated Rubisco content”, and analyzed the correlation between the initial slope of A:Ci and the activated Rubisco content (Figure 7C). The initial slope was highly correlated with activated Rubisco content. Thus, an increase in the Rubisco content and the maintenance of Rubisco activation in RBCS-RCA-ox plants contributed to the enhancement of photosynthesis at moderately high temperatures within the optimal temperature range.

Discussion

Many studies have shown that Rubisco is a primary target for improving photosynthesis. However, our series of studies in transgenic rice plants overproducing Rubisco have shown that the overproduction of Rubisco does not necessarily increase the rate of photosynthesis (Suzuki et al., 2007, 2009). Since a decline in Rubisco activation is associated with the overproduction of Rubisco (Makino and Sage 2007, Suzuki et al., 2009), we produced transgenic rice plants co-overproducing Rubisco and RCA (RBCS-RCA-ox plants). Since our previous studies on RCA-ox plants show that greater than 2-fold increases in the RCA content decrease the Rubisco content (Suganami et al., 2020), there has been a concern that the effect of the Rubisco overproduction in RBCS-ox plants is offset by the overproduction of RCA. However, we successfully produced several lines of RBCS-RCA-ox plants, although some other lines exhibited smaller levels of increase in the Rubisco content (Figure 1 and Supplemental Figure S1). The activation state of Rubisco in all three lines of RBCS-RCA-ox plants was restored to the same level as seen in WT plants (Figure 3). While the rate of CO_2 assimilation at 25°C in RBCS-RCA-ox plants did not

differ from that of WT plants (Figure 4A and Supplemental Figure S2), the rate of CO_2 assimilation at moderately high temperatures under atmospheric CO_2 partial pressures or less was slightly higher in RBCS-ox and RBCS-RCA-ox plants (Figure 5). At 36°C, the initial slope of the A:Ci curve significantly increased in RBCS-RCA-ox plants compared to WT plants, in agreement with an increase in the activated Rubisco content (Figure 7).

As shown in Table 1, the rate of CO_2 assimilation at 25°C is limited by the regeneration capacity of RuBP due to an electron transport limitation. In many plant species, however, the optimal temperature of RuBP regeneration capacity is higher than that of Rubisco-carboxylation capacity (Hikosaka et al., 2006). Therefore, RuBP regeneration capacity is more than the Rubisco-carboxylation capacity at a wide range of moderately high temperatures (Sage and Kubien, 2007). Busch and Sage (2017) identified the photosynthetic limitation by analyzing the sensitivity of O_2 and CO_2 concentrations to photosynthesis and concluded that Rubisco strongly limits photosynthesis at high temperatures. Thus, an increase in CO_2 assimilation at moderately high temperature in RBCS-RCA-ox plants may have been caused by a relative increase in RuBP-regeneration capacity depending on the temperature.

Although the activation state of Rubisco decreases with increasing temperature (Crafts-Brandner and Salvucci, 2000; Makino and Sage, 2007), Yamori et al., (2012) reported that the overproduction of RCA led to a maintenance of the activation state of Rubisco at high temperatures. Similar results were seen for RCA-ox plants in this study (Figure 6B). Although Rubisco activation decreased with temperature in RBCS-RCA-ox plants, the overproduction of RCA restored it

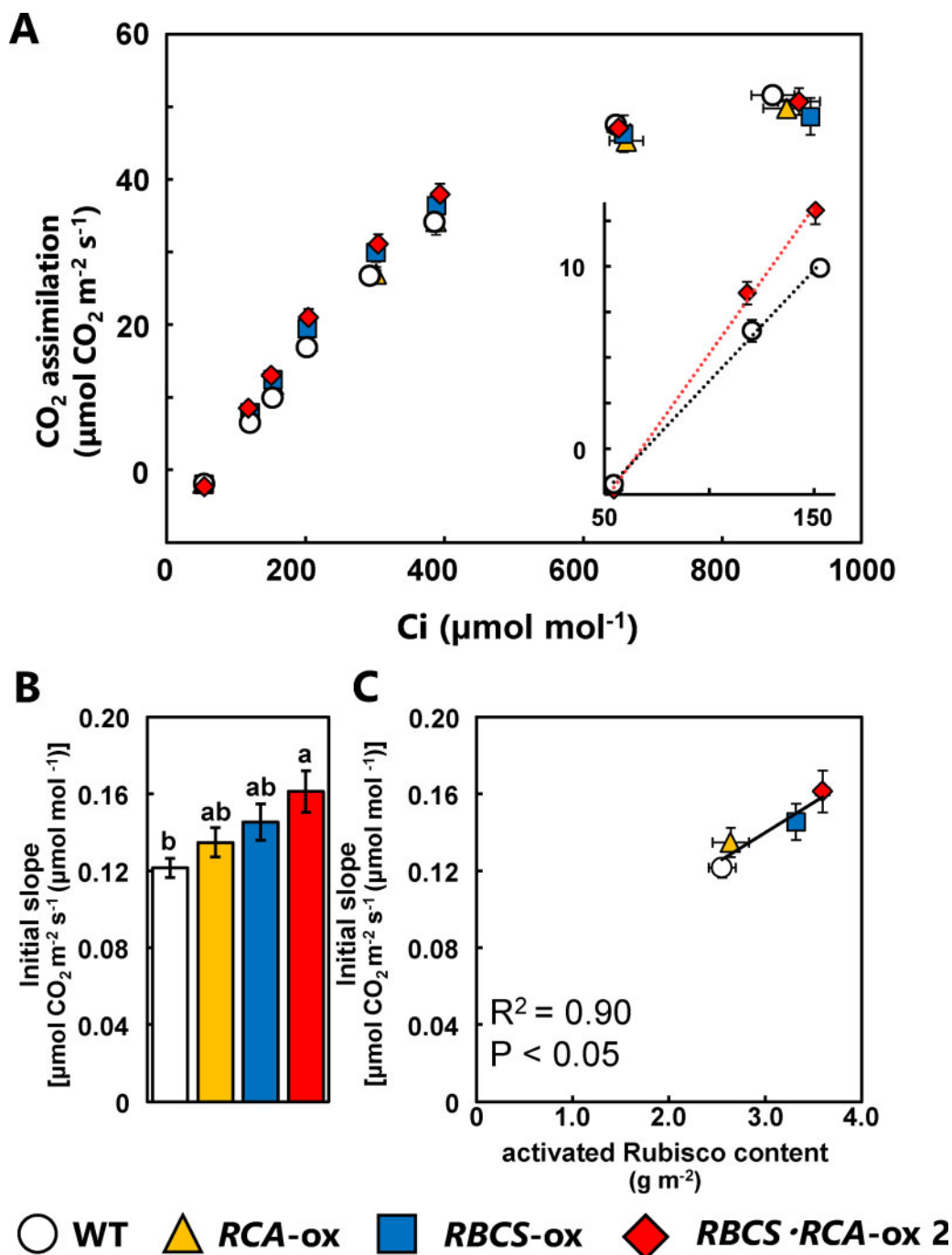


Figure 7 Rates of CO_2 assimilation at 36°C as a function of C_i in transgenic plants. **(A)** $A:C_i$ curve in the uppermost, fully expanded leaves measured with an LI-6800 at a leaf temperature of 36°C and an irradiance of $1,500\text{-}\mu\text{mol quanta m}^{-2}\text{ s}^{-1}$. The white circles, orange triangles, blue squares, and red diamonds indicate WT, RCA-ox, RBCS-ox, and RBCS-RCA-ox 2 plants, respectively. Insert panel **(A)** shows the initial slope of $A:C_i$ curve in WT and RBCS-RCA-ox 2 plants. **(B)** Initial slope of $A:C_i$ curves. The slope was calculated from the data of **(A)**. **(C)** Relationship between the initial slope of $A:C_i$ curve and activated Rubisco content. The activated Rubisco content was calculated by multiplying the Rubisco content by the activation state of Rubisco (Figure 6). The linear regression line was calculated using the Pearson's coefficient of correlation. Data are presented as means \pm SE ($n = 4$). Statistical analysis was conducted using ANOVA with a post hoc Tukey–Kramer HSD test. Different letters indicate statistical differences among the genotypes ($P < 0.05$).

to the same level as seen in WT plants, and Rubisco activation in RBCS-RCA-ox 2 plants was higher than that of RBCS-ox plants at moderately high temperatures (Figure 6B). Therefore, the co-overproduction of Rubisco and RCA

would be effective for an improvement in photosynthesis at moderately high temperatures.

Photosynthetic analysis at 25°C using the C_3 photosynthesis model (Table 1) suggested that the rate of CO_2

assimilation is limited by the electron-transport capacity. However, according to the C_3 photosynthesis model, an increase in the rate of CO_2 assimilation under CO_2 -limited conditions could be expected in *RBCS-RCA-ox* plants, but there was no difference in V_{cmax} and the initial slope of $A:C_i$ between WT and *RBCS-RCA-ox* plants (Table 1 and Figure 4, B and C). We examined the parameters of electron transport around PSII and PSI. No differences in the quantum yield of PSII [$Y(II)$] and nonphotochemical quenching were found among genotypes, irrespective of CO_2 partial pressures (Supplemental Figure S4). These results suggest that there was also no difference in mesophyll conductance between WT and *RBCS-RCA-ox* plants. Therefore, the lack of increase in CO_2 assimilation at $25^\circ C$ under CO_2 -limited conditions in *RBCS-RCA-ox* plants was not caused by the mesophyll conductance. Alternatively, the acceptor-side limitation of PSI [$Y(NA)$] increased, while $Y(I)$ and $Y(ND)$ conversely decreased in *RBCS-RCA-ox* 2 plants (Supplemental Figure S5). However, we are uncertain if such a negative effect on the PSI activity led to no increase in CO_2 assimilation at $25^\circ C$ under CO_2 -limited conditions in *RBCS-RCA-ox* plants. Thus, the reasons for this discrepancy are unknown, but one possibility is that photosynthesis may be coordinated by RuBP regeneration and carboxylation capacities over broad CO_2 partial pressures (Evans, 1986).

We have recently reported that *RBCS-ox* rice plants have greater biomass production and higher yields in an experimental paddy field under sufficient nitrogen fertilization. The rate of CO_2 assimilation in the flag leaf of *RBCS-ox* plants was higher than that of WT plants, which may have resulted in crop productivity improvements (Yoon et al., 2020). Rubisco content in flag leaves of *RBCS-ox* plants grown in the paddy field expressed per unit of land area was 95%–110% greater than that in WT plants under conditions of more than 10 g N m^{-2} nitrogen fertilization. This was much greater than expected based on our previous studies and the present study, all of which were conducted using a growth chamber. Although the difference was mainly caused by greater absorption of nitrogen in *RBCS-ox* plants just before the full-heading stage under sufficient nitrogen conditions, this difference may also be due to higher temperatures in the paddy field during the midsummer than in the growth chamber ($26^\circ C/20^\circ C$ day/night temperature). In addition, the measured temperature of photosynthesis ($33^\circ C$ – $35^\circ C$) was also higher in the field. Since this study showed that *RBCS-RCA-ox* plants exhibited higher photosynthetic capacity than *RBCS-ox* plants at a moderately high temperature within the optimal temperature range, we expect that the *RBCS-RCA-ox* plants have greater biomass production and higher yield capacities in a paddy field.

Conclusion

In this study, we successfully produced transgenic rice plants co-overproducing Rubisco and RCA. The rate of CO_2 assimilation in *RBCS-RCA-ox* plants significantly increased at

moderately high temperatures within the optimal temperature range. Thus, the co-overproduction of Rubisco and RCA could be an efficient strategy to improve photosynthesis and crop productivity. Further studies to evaluate effects of the co-overproduction of Rubisco and RCA on plant biomass and yields at the paddy-field level are in progress.

Materials and methods

Generation of transgenic plants

To produce *RBCS-RCA-ox* plants, two lines of *RBCS*-overexpressing rice (*Oryza sativa*) plants (designated as Sr-26-8 and Sr-35-4 in Suzuki et al., 2007) were crossed with four lines of *RCA*-overexpressing rice plants (designated as Pro_{RBCS} 13, Pro_{RBCS} 5, Pro_{RCA} 42, and Pro_{RCA} 45 in Suganami et al. (2020)). *RCA-ox* plants were transformed with the small form of *RCA* cDNA under the control of the *RBCS2* promoter or the *RCA* promoter. F_1 progenies were selected based on Rubisco and *RCA* contents and allowed to self-fertilize to collect F_2 or F_3 seeds using the Biotron breeding system (Ohnishi et al., 2011). The origins of finally selected lines are summarized in Supplemental Table S1.

Plant culture and sampling

WT rice (*Oryza sativa* L. cv Notohikari), *RBCS-ox* (line Sr-26-8), *RCA-ox* (line Pro_{RBCS} 13), and selected lines of *RBCS-RCA-ox* plants were hydroponically grown in an environmentally controlled growth chamber (type L, NK System, Osaka, Japan) according to Makino et al. (1994) with slight modification as described in Suganami et al. (2018). The chamber was maintained with a 15-h photoperiod, $26^\circ C/20^\circ C$ day/night temperature, and a photosynthetic photon flux density (PPFD) of $1,000 \mu\text{mol quanta m}^{-2} \text{ s}^{-1}$ at daytime. The basal nutrient solution used was described by Makino et al. (1994), and the solution was renewed once a week. In the case of *RBCS-RCA-ox* plants, F_2 or F_3 seeds were used. The selection of homozygotes for *RBCS* and *RCA* transgenes were performed as described by Suzuki et al. (2017). The primer pairs and probes used are summarized in Supplemental Table S2. From the 63–77th day after sowing, the uppermost, fully expanded leaves were used for the measurement of photosynthesis and stored at $-80^\circ C$ until the commencement of biochemical assays. For the mRNA analysis, leaves in the middle of expansion (emerging from their sheath by 60%) and uppermost fully expanded leaves were collected between 11:00 and 13:00 from the 4–7th day following the renewal of the nutrient solution.

Analysis of photosynthesis

The rate of CO_2 assimilation was measured using a portable gas exchange system (LI-6400XT or LI-6800, Li-Cor, Lincoln, NE, USA). Measurements were performed at a $1,500 \mu\text{mol quanta m}^{-2} \text{ s}^{-1}$ PPFD and 1.0 to 1.2 kPa leaf-to-air vapor pressure difference to reach steady-state CO_2 exchange. Gas exchange parameters were calculated according to the equations of von Caemmerer and Farquhar (1981).

The maximum rate of electron transport (J_{\max}) and the maximum rate of RuBP carboxylation (V_{cmax}) were calculated from the equation of von Caemmerer and Farquhar (1981), respectively

$$J_{\max} = (A_{60} + Rd)(4C_c + 8\Gamma^*) / (C_c - \Gamma^*) \quad (1)$$

$$V_{\text{cmax}} = \text{Initial slope of } A : C_c \text{ curve} [C_c + K_c(1 + O/K_o)]^2 / [\Gamma^* + K_c(1 + O/K_o)] \quad (2)$$

where A_{60} is the rate of CO_2 assimilation at $C_i > 60$ Pa, O is the partial pressure of O_2 in the chloroplast (assumed to be the same as in the atmosphere, 21 kPa), K_c and K_o are the Michaelis–Menten constants for CO_2 and O_2 [23.6 Pa and 26.2 kPa, respectively, from rice kinetics data described by Makino et al. (1988)], and Rd is the day respiration [$2.74 \mu\text{mol m}^{-2} \text{s}^{-1}$, from rice grown at 2.0 mM-N described by Yamori et al. (2011)].

The chloroplastic CO_2 partial pressure (C_c) is defined as follows

$$C_c = C_i - A/g_m \quad (3)$$

where g_m is the mesophyll conductance [$0.5 \text{ mol m}^{-2} \text{ s}^{-1}$ from rice data described by von Caemmerer and Evans (1991)]. The CO_2 compensation point of photosynthesis in the absence of Rd (Γ^*) is defined as follows

$$\Gamma^* = 0.5 V_o K_c O / V_c K_o \quad (4)$$

where V_o is the Rubisco activity of oxygenation [$5.7 \text{ mol mol}^{-1} \text{ Rubisco s}^{-1}$, from rice kinetics data described by Makino et al. (1988)].

Electron transport-limited photosynthetic rate (A_j) was calculated from the equation by von Caemmerer and Farquhar (1981)

$$A_j = J_{\max}(C_c - \Gamma^*) / (4C_c + 8\Gamma^*) - Rd \quad (5)$$

Biochemical assay

Total leaf-N, Rubisco, and small-form of RCA (RCA_5) contents were determined on the same leaf. The frozen leaves were homogenized in Na-phosphate buffer (pH 7.0) containing 2-mM iodoacetic acid, 120-mM 2-mercaptoethanol, and 5% (v/v) glycerol. The determination of the total leaf-N and Rubisco contents were performed as described by Makino et al. (1994). Briefly, the total leaf-N content was determined using the Nessler's reagent following Kjeldahl digestion. Rubisco content was determined spectrophotometrically by formamide extraction of Coomassie brilliant blue (CBB) R-250-stained bands corresponding to the large and small subunits of Rubisco, which were separated by SDS-PAGE using calibration curves prepared with purified Rubisco from rice (Makino et al., 1985; <http://prometheuswiki.org/tiki-index.php?page=Rubisco+Determination+by+SDS-PAGE&highlight=Rubisco>). The RCA_5 content was determined by image analysis after SDS-PAGE followed by CBB G-250 staining using calibration curves prepared

with bovine serum albumin, according to Suzuki et al. (2017). Each protein measurement was made with a calibration curve using a standard protein on the same gel.

The activation state of Rubisco was determined as described in Nakano et al. (2000). A leaf blade was illuminated in the chamber of the LI-6800 (conditions; PPFD = $1,500 \mu\text{mol quanta m}^{-2} \text{ s}^{-1}$, $C_a = 40$ Pa) for at least 30 min. After the gas exchange rate had reached the steady-state, the illuminated leaf was immediately frozen in liquid N_2 . The time between interruption of gas exchange conditions and complete freezing was within 2 s. The frozen leaf was quickly extracted within 30 s in 50 mM HEPES (4-(2-hydroxyethyl)-1-piperazineethanesulfonic acid-sodium hydroxide)/NaOH (pH 8.0) containing 20-mM MgCl_2 , 10-mM dithiothreitol, and cOplete, Mini protease inhibitor cocktail (Roche, Mannheim, Germany) after which it was centrifuged at 4°C for 10 s. For the measurement of initial activity, a portion of the supernatant was injected into a reaction mixture of 100-mM HEPES/NaOH (pH 8.0) containing 20-mM MgCl_2 , 5-mM dithiothreitol, 5-mM ATP, 5-mM phosphocreatine, 0.2-mM NADH, 20-mM NaHCO_3 , 0.5-mM ribulose 1,5-bisphosphate (RuBP), 25 U mL^{-1} of glyceraldehyde-3-phosphate dehydrogenase, 25 U mL^{-1} of 3-phosphoglycerate kinase, and 25 U mL^{-1} of creatine phosphokinase. The total activity was measured in the supernatant after incubation with 20-mM NaHCO_3 and 20-mM MgCl_2 . Total activity was measured in the supernatant after sufficient incubation with 20-mM NaHCO_3 and 20-mM MgCl_2 to obtain full activation, and all activities were measured at 25°C .

RNA analysis

Total RNA was extracted according to Suzuki et al. (2004) and Suzuki et al. (2009). The extracted RNA was treated with DNase I (DNA-freeTM DNA Removal Kit, Invitrogen, USA) and then reverse-transcribed (PrimeScriptTM RT Reagent Kit (Perfect Real Time), Takara, Japan) with random hexamers according to the manufacturer's instructions. mRNA levels were determined by reverse transcription quantitative PCR (RT-qPCR) with StepOnePlusTM real-time PCR System v 2.2.2 (Applied Biosystems, USA) and Fast SYBR Green Master Mix (Life Technologies, Japan; Ogawa et al., 2012). As an internal standard, 18S rRNA levels were determined (Supplemental Figure S6). The primer pairs used are summarized in Supplemental Table S3.

Statistical treatments

Data are presented as means \pm SE. Data were statistically analyzed using analysis of variance (ANOVA) followed by the post hoc Tukey–Kramer HSD (honestly significant difference) test ($P < 0.05$). First, one-way ANOVA was used to test for statistically significant differences between means of each trait among the genotypes. If a significant difference ($P < 0.05$) was found, then the post hoc Tukey–Kramer HSD test was performed for multiple pairwise comparisons. The relationship between datasets in Figure 7C was evaluated using Pearson's correlation coefficient. All analyses were conducted using JMP11 (SAS Institute Japan, Tokyo, Japan).

Accession numbers

The sequence date from this article can be found in RAP-DB/GenBank under the following accession numbers: *RBCS2*, Os12g0274700; *RBCS3*, Os12g0291100; *RBCS4*, Os12g0292400; *RBCS5*, Os12g0291400; *RBCL*, OrsajCp033, *RCA*, Os11g0707000.

Supplemental data

The following materials are available in the online version of this article.

Supplemental Figure S1 Detection of Rubisco and RCA proteins in transgenic plants.

Supplemental Figure S2 Rubisco, RCA and leaf-N contents in transgenic plants derived from Sr35-4 lines (*RBCS*-*RCA*-ox plants 4 and 5).

Supplemental Figure S3 Rates of CO₂ assimilation at 25°C in transgenic plants derived from Sr35-4 lines (*RBCS*-*RCA*-ox plants 4 and 5).

Supplemental Figure S4 Chl fluorescence parameters of PSII in transgenic plants.

Supplemental Figure S5 P700 parameters of PSI in transgenic plants.

Supplemental Figure S6 The relative levels of 18S rRNA in transgenic plants.

Supplemental Table S1 Origins of selected *RBCS*-*RCA*-ox lines.

Supplemental Table S2 Primer pairs and probes used for selection of homozygotes.

Supplemental Table S3. Primer pairs used for RT-qPCR analysis.

Supplemental Data Set S1 Source data for Figure 1.

Supplemental Data Set S2 Source data for Figure 2.

Supplemental Data Set S3 Source data for Figure 3.

Supplemental Data Set S4 Source data for Figure 4.

Supplemental Data Set S5 Source data for Figure 5.

Supplemental Data Set S6 Source data for Figure 6.

Supplemental Data Set S7 Source data for Figure 7.

Supplemental Data Set S8 Source data for Table 1.

Acknowledgments

We thank Professor Mitsue Miyao for the use of an LI-6800, and we thank Professors Hiroyuki Ishida and Kouki Hikosaka, and Drs Keiki Ishiyama and Daisuke Takagi, and Mr So Konno for their valuable discussion and comments.

Funding

This work was supported by JSPS KAKENHI (Grant nos. JP16H06379 to A.M. and JP18H02111 to Y.S.), and JSPS Fellowships to M.S. (19J10653), and by JST CREST (Grant no. JPMJCR15O3 to Y.S. and A.M.).

Conflict of interest statement. The authors declare no conflict of interests.

References

- Bracher A, Whitney SM, Hartl FU, Hayer-Hartl M** (2017) Biogenesis and metabolic maintenance of Rubisco. *Annu Rev of Plant Biol* **68**: 29–60
- Busch FA, Sage RF** (2017) The sensitivity of photosynthesis to O₂ and CO₂ concentration identifies strong Rubisco control above the thermal optimum. *New Phytol* **213**: 1036–1051
- Carmo-Silva AE, Salvucci ME** (2013) The regulatory properties of Rubisco activase differ among species and affect photosynthetic induction during light transitions. *Plant Physiol* **161**: 1645–1655
- Carmo-Silva AE, Scales JC, Madgwick PJ, Parry MA** (2015) Optimizing Rubisco and its regulation for greater resource use efficiency. *Plant Cell Environ* **38**: 1817–1832
- Crafts-Brandner SJ, Salvucci ME** (2000) Rubisco activase constrains the photosynthetic potential of leaves at high temperature and CO₂. *Proc Natl Acad Sci USA* **97**: 13430–13435
- Eckardt NA, Snyder GW, Portis AR, Ogren WL** (1997) Growth and photosynthesis under high and low irradiance of *Arabidopsis thaliana* antisense mutants with reduced ribulose-1,5-bisphosphate carboxylase/oxygenase activase content. *Plant Physiol* **113**: 575–586
- Evans JR** (1986) The relationship between carbon-dioxide-limited photosynthetic rate and ribulose-1,5-bisphosphate-carboxylase content in two nuclear-cytoplasm substitution lines of wheat, and the coordination of ribulose-bisphosphate-carboxylation and electron-transport capacities. *Planta* **167**: 351–358
- Farquhar GD, von Caemmerer S, Berry JA** (1980) A biochemical model of photosynthetic CO₂ assimilation in leaves of C₃ species. *Planta* **149**: 78–90
- Fukayama H, Ueguchi C, Nishikawa K, Katoh N, Ishikawa C, Masumoto C, Hatanaka T, Misoo S** (2012) Overexpression of Rubisco activase decreases the photosynthetic CO₂ assimilation rate by reducing Rubisco content in rice leaves. *Plant Cell Physiol* **53**: 976–986
- Furbank RT, Chitty JA, von Caemmerer S, Jenkins C** (1996) Antisense RNA inhibition of *RbcS* gene expression reduces Rubisco level and photosynthesis in the c4 plant *Flaveria bidentis*. *Plant Physiol* **111**: 725–734
- Hikosaka K, Ishikawa K, Borjigidai A, Muller O, Onoda Y** (2006) Temperature acclimation of photosynthesis: mechanisms involved in the changes in temperature dependence of photosynthetic rate. *J Exp Bot* **57**: 291–302
- Hudson GS, Evans JR, von Caemmerer S, Arvidsson YB, Andrews TJ** (1992) Reduction of ribulose-1,5-bisphosphate carboxylase/oxygenase content by antisense RNA reduces photosynthesis in transgenic tobacco plants. *Plant Physiol* **98**: 294–302
- IPCC (2013) Working group I contribution to the IPCC fifth assessment report climate change 2013. *In* The Physical Science Basis Summary for Policymakers. IPCC, Geneva
- Long SP, Marshall-Colon A, Zhu XG** (2015) Meeting the global food demand of the future by engineering crop photosynthesis and yield potential. *Cell* **161**: 56–66
- Makino A** (2011) Photosynthesis, grain yield, and nitrogen utilization in rice and wheat. *Plant Physiol* **155**: 125–129
- Makino A, Mae T, Ohira K** (1985) Enzymic properties of ribulose-1,5-bisphosphate carboxylase/oxygenase purified from rice leaves. *Plant Physiol* **79**: 57–61
- Makino A, Mae T, Ohira K** (1988) Differences between wheat and rice in the enzymic properties of ribulose-1,5-bisphosphate carboxylase/oxygenase and the relationship to photosynthetic gas exchange. *Planta* **174**: 30–38
- Makino A, Nakano H, Mae T** (1994) Responses of ribulose-1,5-bisphosphate carboxylase, cytochrome-*f*, and sucrose synthesis enzymes in rice leaves to leaf nitrogen and their relationships to photosynthesis. *Plant Physiol* **105**: 173–179
- Makino A, Sage RF** (2007) Temperature response of photosynthesis in transgenic rice transformed with ‘sense’ or ‘antisense’ *rbcS*. *Plant Cell Physiol* **48**: 1472–1483

- Makino A, Shimada T, Takumi S, Kaneko K, Matsuoka M, Shimamoto K, Nakano H, Miyao-Tokutomi M, Mae T, Yamamoto N** (1997) Does decrease in ribulose-1,5-bisphosphate carboxylase by antisense *RbcS* lead to a higher N-use efficiency of photosynthesis under conditions of saturating CO₂ and light in rice plants? *Plant Physiol* **114**: 483–491
- Masumoto C, Fukayama H, Hatanaka T, Uchida N** (2012) Photosynthetic characteristics of antisense transgenic rice expressing reduced levels of Rubisco activase. *Plant Prod Sci* **15**: 174–182
- Mate CJ, von Caemmerer S, Evans JR, Hudson GS, Andrews TJ** (1996) The relationship between CO₂-assimilation rate, Rubisco carbamylation and Rubisco activase content in activase-deficient transgenic tobacco suggests a simple model of activase action. *Planta* **198**: 604–613
- Nakano H, Muramatsu S, Makino A, Mae T** (2000) Relationship between the suppression of photosynthesis and starch accumulation in the pod-removed bean. *Aust J Plant Physiol* **27**: 167–173
- Nagai T, Makino A** (2009) Differences between rice and wheat in temperature responses of photosynthesis and plant growth. *Plant Cell Physiol* **50**: 744–755
- Ogawa S, Suzuki Y, Yoshizawa R, Kanno K, Makino A** (2012) Effect of individual suppression of *RBCS* multigene family on Rubisco contents in rice leaves. *Plant Cell Environ* **35**: 546–553
- Ohnishi T, Yoshino M, Yamakawa H, Kinoshita T** (2011) The biotron breeding system: a rapid and reliable procedure for genetic studies and breeding in rice. *Plant Cell Physiol* **52**: 1249–1257
- Ort DR, Merchant SS, Alric J, Barkan A, Blankenship RE, Bock R, Croce R, Hanson MR, Hibberd JM, Long SP, et al.** (2015) Redesigning photosynthesis to sustainably meet global food and bioenergy demand. *Proc Natl Acad Sci USA* **112**: 8529–8536
- Parry MA, Keys AJ, Madgwick PJ, Carmo-Silva AE, Andralojc PJ** (2008) Rubisco regulation: a role for inhibitors. *J Exp Bot* **59**: 1569–1580
- Portis AR** (2003) Rubisco activase – Rubisco’s catalytic chaperone. *Photosynth Res* **75**: 11–27
- Quick WP, Schurr U, Scheibe R, Schulze ED, Rodermel SR, Bogorad L, Stitt M** (1991) Decreased ribulose-1,5-bisphosphate carboxylase-oxygenase in transgenic tobacco transformed with “antisense” *rbcS*. I. Impact on photosynthesis in ambient growth-conditions. *Planta* **183**: 542–554
- Sage RF, Kubien DS** (2007) The temperature response of C₃ and C₄ photosynthesis. *Plant Cell Environ* **30**: 1086–1106
- Salesse-Smith CE, Sharwood RE, Busch FA, Kromdijk J, Bardal V, Stern DB** (2018) Overexpression of Rubisco subunits with RAF1 increases Rubisco content in maize. *Nat Plants* **4**: 802–810
- Sudo E, Suzuki Y, Makino A** (2014) Whole-plant growth and N utilization in transgenic rice plants with increased or decreased Rubisco content under different CO₂ partial pressures. *Plant Cell Physiol* **55**: 1905–1911
- Suganami M, Suzuki Y, Kondo E, Nishida S, Konno S, Makino A** (2020) Effects of overproduction of Rubisco activase on Rubisco content in transgenic rice grown at different N levels. *Int J Mol Sci* **21**: 1626
- Suganami M, Suzuki Y, Sato T, Makino A** (2018) Relationship between Rubisco activase and Rubisco contents in transgenic rice plants with overproduced or decreased Rubisco content. *Soil Sci Plant Nutr* **64**: 352–359
- Suzuki Y, Fujimori T, Kanno K, Sasaki A, Ohashi Y, Makino A** (2012) Metabolome analysis of photosynthesis and the related primary metabolites in the leaves of transgenic rice plants with increased or decreased Rubisco content. *Plant Cell Environ* **35**: 1369–1379
- Suzuki Y, Kawazu T, Koyama H** (2004) RNA isolation from siliques, dry seeds, and other tissues of *Arabidopsis thaliana*. *Biotechniques* **37**: 542–544
- Suzuki Y, Kondo E, Makino A** (2017) Effects of co-overexpression of the genes of Rubisco and transketolase on photosynthesis in rice. *Photosynth Res* **131**: 281–289
- Suzuki Y, Makino A** (2012) Availability of Rubisco small subunit up-regulates the transcript levels of large subunit for stoichiometric assembly of its holoenzyme in rice. *Plant Physiol* **160**: 533–540
- Suzuki Y, Miyamoto T, Yoshizawa R, Mae T, Makino A** (2009) Rubisco content and photosynthesis of leaves at different positions in transgenic rice with an overexpression of *RBCS*. *Plant Cell Environ* **32**: 417–427
- Suzuki Y, Ohkubo M, Hatakeyama H, Ohashi K, Yoshizawa R, Kojima S, Hayakawa T, Yamaya T, Mae T, Makino A** (2007) Increased Rubisco content in transgenic rice transformed with the ‘sense’ *rbcS* gene. *Plant Cell Physiol* **48**: 626–637
- To KY, Suen, DF, Grace-Chen SC** (1999) Molecular characterization of ribulose-1,5-bisphosphate carboxylase/oxygenase in rice leaves. *Planta* **209**: 66–76
- von Caemmerer S** (2020) Rubisco carboxylase/oxygenase: from the enzyme to the globe: a gas exchange perspective. *J Plant Physiol* **252**: 153240
- von Caemmerer S, Evans J** (1991) Determination of the average partial pressure of CO₂ in chloroplasts from leaves of several C₃ plants. *Aust J Plant Physiol* **18**: 287–305
- von Caemmerer S, Farquhar GD** (1981) Some relationships between the biochemistry of photosynthesis and the gas exchange of leaves. *Planta* **153**: 376–387
- Wada S, Suzuki Y, Takagi D, Miyake C, Makino A** (2018) Effects of genetic manipulation of the activity of photorespiration on the redox state of photosystem I and its robustness against excess light stress under CO₂-limited conditions in rice. *Photosynth Res* **137**: 431–441
- Yamori W, Masumoto C, Fukayama H, Makino A** (2012) Rubisco activase is a key regulator of non-steady-state photosynthesis at any leaf temperature and, to a lesser extent, of steady-state photosynthesis at high temperature. *Plant J* **71**: 871–880
- Yamori W, Nagai T, Makino A** (2011) The rate-limiting step for CO₂ assimilation at different temperatures is influenced by the leaf nitrogen content in several C₃ crop species. *Plant Cell Environ* **34**: 764–777
- Yoon D-K, Ishiyama K, Suganami M, Tazoe Y, Watanabe M, Imaruoka S, Ogura M, Ishida H, Suzuki Y, Obara M, et al.** (2020) Transgenic rice overproducing Rubisco exhibits increased yields with improved nitrogen-use efficiency in an experimental paddy field. *Nature Food* **1**: 134–139
- Zhang N, Kallis RP, Ewy RG, Portis AR Jr.** (2002) Light modulation of Rubisco in *Arabidopsis* requires a capacity for redox regulation of the larger Rubisco activase isoform. *Proc Natl Acad Sci USA* **99**: 3330–3334
- Zhang N, Portis AR Jr.** (1999) Mechanism of light regulation of Rubisco: a specific role for the larger Rubisco activase isoform involving reductive activation by thioredoxin-f. *Proc Natl Acad Sci USA* **96**: 9438–9443